International Journal of Thermal Sciences 86 (2014) 387–393

Contents lists available at ScienceDirect

International Journal of Thermal Sciences

journal homepage: www.elsevier.com/locate/ijts

The thermoelectric figure of merit for the single electron transistor

E. Ramos [a], J. Silva-Valencia [a], R. Franco [a, *], M.S. Figueira [b]

[a] Departamento de Física, Universidad Nacional de Colombia, A.A. 5997, Bogotá, Colombia
[b] Instituto de Física, Universidade Federal Fluminense, Av. Litorânea s/n, 24210-346 Niterói, Rio de Janeiro, Brazil

ARTICLE INFO

Article history:
Received 20 January 2014
Received in revised form
26 June 2014
Accepted 27 July 2014
Available online 28 August 2014

Keywords:
Single electron transistor
Thermoelectric figure of merit
Atomic approach

ABSTRACT

We study the thermoelectric transport properties of a single electron transistor. We describe a two-level quantum dot, connected to right and left leads, employing the single impurity Anderson model with local finite electronic correlation. Using the linear response theory, we compute the thermoelectric transport coefficients. We calculate the thermoelectric properties employing the Green's functions calculated within the atomic approach, but for simplicity, we only consider the electronic contribution and neglect the phononic contribution to the thermal conductance. In the single electron transistor this is not so drastic, because the phononic contribution can be minimized, isolating the quantum dot from the electrodes with two tunneling barriers, whose material can be appropriately chosen to produce a low phononic contribution. We show that the best dimensionless thermoelectric figure of merit for the single electron transistor, occurs in the weak coupling regime, at temperatures well above the Kondo temperature.

1. Introduction

The development of semiconductor technology in the 1950's, with the discovery that heavily doped semiconductors and the compound Bi_2Te_3 are good thermoelectric materials, gave rise to the modern thermoelectric industry, with the development of new commercial power generation and cooling systems. During the next three decades, with little interest from the scientific community, the thermoelectric field developed slowly. But at the beginning of the 1990's, after the publication of two important papers by L.D. Hicks and M. S. Dresselhaus [1], the situation changed completely. They suggested that the quantum confinement present in low dimensional systems could be employed for engineering the thermoelectric properties of those materials. In the wake of these papers, an intense effort was made to explore the new routes opened by the experimental achievements in nanoscopic systems research, such as quantum dots, nanowires, quantum wells, superlattices, and more recently nanocomposite materials. A critical discussion of the development of this important area can be found in some recent reviews [2.3,4,5,6].

During the last 10 years, several experimental setups for exploring the thermoelectric properties of nanoscopic systems [7–11] have opened up the possibility of using such systems for controlling the energy transport on a microscopic scale. In a recent experiment, a gate-controlled single-electron refrigerator was obtained, in which the Coulomb correlation controls the heat transfer and, the refrigeration process in a mesoscopic system [12]. In another interesting paper, Popescu et al. [13], investigated the fundamental dimensional limits for thermodynamic machines and showed that it was possible to construct self-contained refrigerators (i.e., not requiring external sources of work) consisting of only a small number of qubits and/or qutrits. Another paper related to our calculations was the study of thermoelectric effects in molecular junctions by Pramod Reddy et al. [14], who trapped molecules between two gold electrodes with a temperature difference across them. From the theoretical point of view we can refer two recent papers employing the numerical renormalization group [15,16].

A strong motivation for studying the single electron transistor (SET) is that this system is the experimental realization of the single impurity Anderson model (SIAM) for finite electronic correlation *U*. The SIAM was experimentally realized by the Goldhaber-Gordon group [17] with complete control over all the parameters of the model. They measured the electric conductance of a SET and showed its universal character.

* Corresponding author.
E-mail addresses: rfrancop@unal.edu.co, robertofrancop@gmail.com (R. Franco), figueira@if.uff.br (M.S. Figueira).

http://dx.doi.org/10.1016/j.ijthermalsci.2014.07.018
1290-0729/

Nomenclature

Constants

k_B	Boltzmann constant = 1.38×10^{-23} m^2 Kg s^{-2}
e	electron charge = 1.6×10^{-19} C

Symbols

e	electron charge, C
μ	chemical potential, J
V	hybridization, J
U	correlation energy, J
E_{QD}	quantum dot energy, J
D	semi-width conduction band, J
Γ	energy unit, J
Δ	Anderson parameter, J
n_F	Fermi-Dirac distribution,
K_e	electronic thermal conductance, W m^{-2} K^{-1}
K_{ph}	phonon thermal conductance, W m^{-2} K^{-1}
I_o,I_1,I_2	transport coefficients,
L_o	Lorenz number, W Ω K^{-2}
S	Thermopower, V K^{-1}
T	temperature, K
ZT	dimensionless thermoelectric figure of merit,
G	electrical conductance, C^2 Kg^{-1} m^{-2} s^{-1}
ω	energy, J
Ω	thermodynamical potential, J

The dimensionless thermoelectric figure of merit ZT indicates the system performance. It constitutes a measure of the usefulness of materials or devices to be employed for thermopower generators or cooling systems, and is defined by.

$$\mathrm{ZT} = S^2 \mathrm{TG} \Big/ K, \tag{1}$$

where G is the electrical conductance, S is the thermoelectric power, K is the thermal conductance and T is the absolute temperature. If ZT > 1, the system is considered to be a possible candidate for technological applications. In ordinary metals, the thermal and electrical conductances are related to the same scattering processes, with only weak energy dependence. This is the main reason why metals show lower dimensionless thermoelectric figure of merit ZT values. After the discovery in the fifties, that the alloys of Bi_2Te_3 exhibit ZT ≃ 1, near room temperature, this compound has dominated the whole field of thermoelectric materials up until today. All efforts to increase the ZT values have resulted in few advances, due to the interdependence between the physical properties associated with ZT. A summary of the evolution of ZT values can be found in Fig. 1 of the C. J. Vineis et al. review [4]. However, nanoscopic systems open up new possibilities for increasing ZT, mainly due to the level quantization and the Coulomb interaction, which could lead to important changes in the thermoelectric properties of the system.

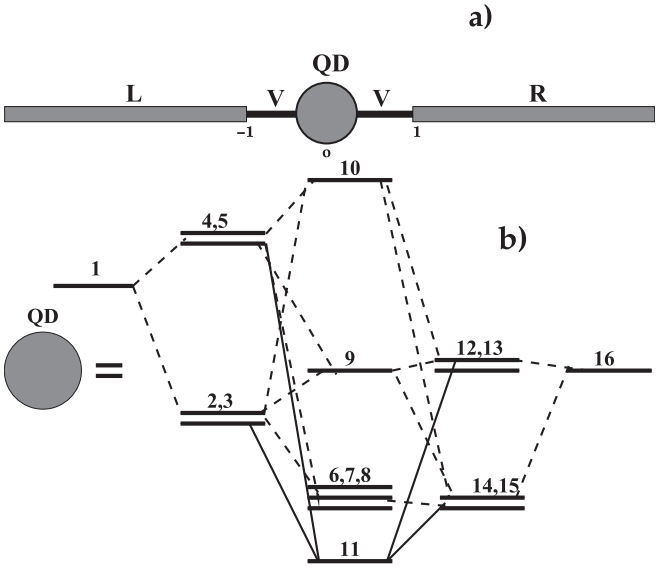

Fig. 1. (a) Schematic picture of the SET. A quantum dot embedded into conduction leads and (b) Details of the eigen states structure of the atomic solution generated through the atomic approach in the Kondo regime.

In the present paper, we show that the violation of the Wiedemann-Franz law (WF) within the temperature interval $k_BT = [1–5]\Gamma$, where k_B is the Boltzmann constant, is associated with a strong increase in the dimensionless thermoelectric figure of merit ZT. Γ is an energy unit associated with the energy width of the conduction band. We assume a flat density of states of magnitude $\rho_c = 1/2D$ per spin channel for both leads, where we employ the energy unit $\Gamma = 1$ with $D = 100\Gamma$ being the half bandwidth of each lead. To simplify the notation we set. $k_B = 1$.

The conductance unitary limit is experimentally attained in real quantum dot (QD) systems, at temperatures on the order of 10 mK. W. G. van der Wiel *et al.* [18] obtained the unitary limit in a semiconductor QD at $T = 15$ mK with an applied magnetic field of $B = 0.4T$, and A. V. Kretinin *et al.* [19] obtained the same limit in a suspended nanowire-based QD device, at temperature $T = 10$ mK. In their setup, there is no applied magnetic field. Since in our units, the unitary limit of the conductance was attained at $T = 10^{-3}\Gamma$ (these results are not shown here), we estimate $\Gamma \simeq 10$ K, and since we are studying the temperature region $T = [1–5]\Gamma$ where charge fluctuations becomes important, we estimate that in real systems, those temperatures will occur approximately within the range of $T \simeq [10–50]$ K, which is easily attained in a liquid helium cryostat.

In a general way, G.D. Mahan and J. O. Sofo [20] discussed, the conditions that a device must fulfill in order to produce the best thermoelectric efficiency. They investigated what type of electronic structure provides the largest dimensionless thermoelectric figure of merit for thermoelectric materials. They determined that a narrow energy distribution of the carriers was needed in order to produce a large value of ZT. In the present paper, we show that this general condition is fulfilled by the SET at the weak coupling limit (low hybridizations values) and within the temperature range $T \simeq [10–50]$ K, above the Kondo temperature. The regions where ZT exhibits high values corresponds to the transition from the empty dot to the intermediate valence and the transition from the singly to the doubly occupied states. We show that this is the most interesting region, because ZT attains strong values.

Considering the electronic and phononic contributions separately, ZT, can be written as.

$$\mathrm{ZT} = S^2 \mathrm{TG} \Big/ \left(K_e + K_{\mathrm{ph}}\right). \tag{2}$$

where K_e and K_{ph} are the electronic and the phononic contribution to the thermal conductance, respectively.

In low dimensional structures, such as films, wires, and superlattices, the large values of the phononic contribution attained by K_{ph} is responsible for low ZT values [21]. In the SET, the phononic contribution to thermal conductance can be minimized, because the QD is isolated from the electrodes by two tunneling barriers, whose material can be appropriately chosen to produce low K_{ph} values or by alloying the barriers material in order to introduce atomic scale defects and scatter phonons [4]. However, since we are working at temperatures within the interval $T=[1-5]\Gamma$, we believe that the increase of the phononic contribution is important for diminishing the strong ZT increase due to electrons.

Taking into account that usually a SET is basically a lithographic nanostructure obtained over a $GaAs_{(1-x)}Al_x$–GaAs quantum well [7–9,17], where electrons and holes are confined in a two dimensional gas, and the substrate that "supports" the two dimensional gas consists of two $GaAs_{(1-x)}Al_x$ bulk pieces, each one with a Debye temperature $T_D \simeq 300$ K [22], and since our estimation of the temperature interval is $T=[1-5]\Gamma \simeq [10-50]$ K, we confirmed that the temperature values are below the value of the Debye temperature of the substrates, as a consequence, we expected that the phononic contribution of the substrates would be low. Recently, new research has been published that takes into consideration the phononic contribution to the thermal conductivity. That most similar to the present paper is that of Jie Ren et al. [23]. However, in order to include phonons we need to reformulate the atomic approach which can make the calculations very complicated, and for the sake of simplicity, we do not consider the phononic contribution to the thermal conductivity K_{ph} in the present paper, but rather we indicate its main effect on the thermoelectric properties.

We organize this paper in the following way: In Section 2, we define the model in terms of the X Hubbard operators. In Section 3, we present a brief review of the main equations employed in the calculation of the Green's functions by the atomic approach. In Section. 4, we discuss the thermoelectric properties. In Section 5, we present the results of our research and discuss their physical consequences. Finally, in Section 6, we present a summary of the main results obtained as well as the conclusions of the paper.

2. Model and theory

In Fig. 1a, we present a pictorial view of the SET considered in the present paper. In Fig. 1b, we represent the eigen states of the atomic solution, which are the "seed" employed to calculate the Green's functions of the atomic approach. Those Green's functions have the general form [24]:

$$g_\sigma^{f,\mathrm{at}}(\omega) = e^{\beta\Omega}\sum_{i=1}^{16}\frac{m_i}{\omega-u_i}, \tag{3}$$

where Ω is the thermodynamic potential, the poles u_i in the denominator, are the energy eigenvalues associated with the energy levels, and the residues m_i in the numerator, are the occupation numbers associated with the atomic transitions. In the diagram, we indicate, transitions with null residues ($m_i=0$), with dashed lines and transitions with non null residues ($m_i\neq 0$) with solid lines, but as the temperature or the other parameters of the model change, the residues of the Green's functions change as well and the dotted lines can become solid lines and vice-versa. The resultant eigen state structure of the QD corresponds to the atomic solution of the periodic Anderson model (PAM), (For more details cf. Fig. 20 and the appendix of Ref. [24]).

This particular eigen state structure corresponds to the Kondo limit at a temperature T, below the Kondo temperature T_K. The Kondo singlet ground state is given by the level 11, and the transitions represented by the full lines produce non null residues for the atomic Green's functions, which give rise to the Kondo peak. The transitions represented by dashed lines vanish in the Kondo region, but become important in the temperature region, where we obtain high ZT values. This QD eigen state structure is not static, but rather changes with temperature and the QD localized energy level $E_{f\sigma}$, follows the different regimes of the SIAM: empty dot, intermediate valence, Kondo, and double occupation.

The Hamiltonian of the system can be written as.

$$H=\sum_{\alpha=L,R}\sum_{\mathbf{k},\sigma}E^{\alpha}_{\mathbf{k},\sigma}c^{\alpha\dagger}_{\mathbf{k},\sigma}c^{\alpha}_{\mathbf{k},\sigma}+\sum_{\sigma}\left[E_{f\sigma}X_{\sigma\sigma}+\left(E_{f\sigma}+U\right)X_{\mathrm{dd}}\right] + \sum_{\alpha=L,R}\sum_{\mathbf{k},\sigma}V_\alpha\left(X^{\dagger}_{0\sigma}c^{\alpha}_{\mathbf{k},\sigma}+c^{\alpha\dagger}_{\mathbf{k},\sigma}X_{0\sigma}\right), \tag{4}$$

where the first term represents the leads, characterized by free conduction electrons (c-electrons) to the right (R) and to the left (L) of the QD (Fig. 1a). The second term describes the QD defined by a two-level structure: one localized (f-electrons) bare level $E_{f\sigma}=E_{QD}$ and the local Coulomb interaction of the QD, characterized by the double occupation level at $E_{QD}+U$ [24,25]. These localized levels are expressed in the representation of Hubbard operators, which are convenient for working with correlated local states and are defined in general by $X_{p,ab}=|p,a><p,b|$.We would like to mention that the simple two-level structure of the isolated QD, is changed when this QD is allowed to interact with the conduction electron band. This simple structure is modified by the interaction and the atomic approach changes it, into the "atomic eigen state structure" represented in Fig. 1b. The third term corresponds to the tunneling between the embedded dot and the left (L) and right (R) semi-infinite leads. The amplitude V_α is responsible for the tunneling between the QD and the lead α. For simplicity, we assume symmetric junctions (i.e. $V_\alpha=V_L=V_R=V$) and identical leads connecting the QD to the quantum wire.

We solve the Hamiltonian employing the atomic approach for the finite correlation U case. This method was developed in earlier papers [24,25], and here we present a short review of it in Section 4. The atomic approach is able to capture the low temperature physics, dominated by the Kondo effect as well as the region $T\geq\Gamma$, where charge fluctuation processes are dominant. In that temperature region, the dimensionless thermoelectric figure of merit ZT attains values greater than the unit, in the transition from the empty dot to the intermediate valence regions.

3. The atomic approach for the single impurity Anderson model (SIAM)

In previous papers [24,25], one of us developed a simple method, that employs the atomic solution of the periodic Anderson model as a "seed", for generating approximate Green's functions for describing the Kondo physics of strongly correlated electron systems.

The exact GF for the f electrons, which is valid both for the PAM and the SIAM, can be written in the form of a Dyson equation [24]

$$\mathbf{G}^f_\sigma=\mathbf{M}_\sigma\cdot(\mathbf{I}-\mathbf{A}_\sigma)^{-1}, \tag{5}$$

where $\mathbf{A_\sigma}=\mathbf{W}_\sigma\cdot\mathbf{M}_\sigma$ and $\mathbf{M}_\sigma$ are the exact effective cumulants. Inverting Eq. (5), we obtain

$$\mathbf{M}_\sigma=\left(\mathbf{I}+\mathbf{G}^f_\sigma\cdot\mathbf{W}_\sigma\right)^{-1}\cdot\mathbf{G}^f_\sigma, \tag{6}$$

and for an impurity located at the origin $\mathbf{W}_\sigma$ is given by.

$$\mathbf{W}_{\uparrow}(z) = |V|^2 \varphi_{\uparrow}(z)\mathbf{I}, \tag{7}$$

$$\mathbf{W}_{\downarrow}(z) = |V|^2 \varphi_{\downarrow}(z)\mathbf{I}', \tag{8}$$

where

$$\mathbf{I} = \begin{pmatrix} 1 & 1 \\ 1 & 1 \end{pmatrix} \quad , \quad \mathbf{I}' = \begin{pmatrix} 1 & -1 \\ -1 & 1 \end{pmatrix}. \tag{9}$$

For a rectangular band with half-width D in the interval $[-D,D]$, we have.

$$\varphi_{\sigma}(z) = \frac{-1}{2D} \ln\left(\frac{z+D+\mu}{z-D+\mu}\right), \tag{10}$$

where μ is the chemical potential.

Since the calculation of the exact effective cumulant $\mathbf{M}_{\sigma}$ is equivalent to obtaining the exact Green's functions [24,25], we introduce an approximation that consists of substituting the exact effective cumulant in the Green's functions with the approximated ones, obtained from the atomic solution of the model, which is associated with the transitions described by the Hubbard operators. We employ the index $I_x = 1,2,3,4$, defined in Table 1, to characterize these X operators:

In the atomic approach, those approximated GF's become.

$$\mathbf{G}^{f}_{\uparrow}(i\omega) = \frac{\mathbf{M}^{\mathbf{at}}_{13}(i\omega) - |V|^2 \varphi_{\uparrow}(i\omega) R^{13}\mathbf{I}'}{1 - |V|^2 \varphi_{\uparrow}(i\omega) S^{13}}, \tag{12}$$

with $R^{13} = m_{11}m_{33} - m_{13}m_{31}$ and. $S^{13} = m_{11} + m_{33} + m_{13} + m_{31}$

$$\mathbf{G}^{f}_{\downarrow}(i\omega) = \frac{\mathbf{M}^{\mathbf{at}}_{24}(i\omega) - |V|^2 \varphi_{\downarrow}(i\omega) R^{24}\mathbf{I}}{1 - |V|^2 \varphi_{\downarrow}(i\omega) S^{24}}, \tag{13}$$

with $R^{24} = m_{22}m_{44} - m_{24}m_{42}$ and $S^{24} = m_{22} + m_{44} + m_{24} + m_{42}$ and.

$$\mathbf{M}^{\mathbf{at}}_{13}(i\omega) = \begin{pmatrix} m^{\mathrm{at}}_{11} & m^{\mathrm{at}}_{13} \\ m^{\mathrm{at}}_{31} & m^{\mathrm{at}}_{33} \end{pmatrix}, \tag{14}$$

$$\mathbf{M}^{\mathbf{at}}_{24}(i\omega) = \begin{pmatrix} m^{\mathrm{at}}_{22} & m^{\mathrm{at}}_{24} \\ m^{\mathrm{at}}_{42} & m^{\mathrm{at}}_{44} \end{pmatrix} \tag{15}$$

are the atomic cumulants calculated from the atomic Green's functions (For more details cf. section III and the appendix of our Ref. [24]). In the same way, we can obtain the conduction $\mathbf{G}^{\mathrm{cc}}_{\sigma}(\mathbf{k},\mathbf{k}',i\omega)$ and the cross $\mathbf{G}^{\mathrm{cf}}_{\sigma}(\mathbf{k},i\omega)$ Green's functions.

The exact atomic Green's function $g^{f,\mathrm{at}}_{\sigma}(z)$ of the atomic problem satisfies a Dyson equation of the same form as Eq. (5), but now in terms of the atomic cumulants given by Eqs. (14) and (15).

$$\mathbf{g}^{f,\mathrm{at}}_{\sigma} = \mathbf{M}^{\mathbf{at}}_{\sigma} \cdot \left(\mathbf{I} - \mathbf{W}^{\mathbf{o}}_{\sigma}\mathbf{M}^{\mathbf{at}}_{\sigma}\right)^{-1}. \tag{16}$$

It should be stressed that $\mathbf{g}^{f,\mathrm{at}}_{\sigma}$ is known and it is obtained from the exact analytical diagonalization of a 16 × 16 matrix, which represents the atomic solution of the periodic Anderson Hamiltonian (For more details cf. the appendix of our reference [24]). From this equation we obtain the exact atomic cumulant. $\mathbf{M}^{\mathrm{at}}_{\sigma}$

$$\mathbf{M}^{\mathrm{at}}_{\sigma} = \left(\mathbf{I} + \mathbf{g}^{f,\mathrm{at}}_{\sigma} \cdot \mathbf{W}^{o}_{\sigma}\right)^{-1} \cdot \mathbf{g}^{f,\mathrm{at}}_{\sigma}, \tag{17}$$

where

$$\mathbf{W}^{o}_{\uparrow}(z) = |\Delta|^2 \varphi^{o}_{\uparrow}(z) \; ; \; \mathbf{W}^{o}_{\downarrow}(z) = |\Delta|^2 \varphi^{o}_{\downarrow}(z)\mathbf{I}, \tag{18}$$

and.

$$\varphi^{o}_{\sigma}(z) = \frac{-1}{z - \varepsilon_o - \mu}. \tag{19}$$

This equation corresponds to the zero-width band located at ε_0, namely the bare conduction Green's function. The atomic cumulant M^{at}_{σ}, (Eq. (17)) is obtained by replacing Eqs. (18)-19) in Eq. (17). The full Green's functions $\mathbf{G}^{f}_{\sigma}$ are calculated by substituting the cumulants obtained in this way in Eqs. (12) and (13). This procedure overestimates the contribution of the c electrons, because we concentrate them at a single energy level ε_o, and to moderate this effect we replace V^2 in Eq. (18), with the Anderson parameter $\Delta = \pi V^2 \rho_c(\mu) = \pi V^2/2D$.

We should stress that in the low temperature regime the atomic approach imposes the fulfillment of the Friedel sum rule, but for temperatures above the Kondo temperature T_K, as happens in the present paper for $T \simeq \Gamma$, we do not apply this procedure; we only put the conduction atomic level of Eq. (19) at the chemical potential position, $\varepsilon_0 = \mu$.

Table 1
Representation of the possible transitions present in the finite U atomic SIAM Hamiltonian. $I_x = 1,3$ destroys one electron with spin up, and $I_x = 2,4$ destroys one electron with spin down.

I_x	1	2	3	4
$\alpha = (b,a)$	$(0,\uparrow)$	$(0,\downarrow)$	$(\downarrow,d)$	$(\uparrow,d)$

(11)

4. Thermoelectric properties

For ordinary metals, the Wiedemann-Franz (WF) law states that the relation between the electronic contribution to the thermal conductance K_e and the product of the temperature T and the electrical conductance G.

$$\mathrm{WF} = \frac{K_e(T)}{\mathrm{TG}(T)}, \tag{20}$$

is independent of temperature and assumes a universal value given by the Lorenz number [16], $L_o = (\pi^2/3)(k_B/e)^2$, where k_B is the Boltzmann constant and e is the electron charge. In our calculations, we employ WF defined in terms of L_o units.

Combining Eqs. (1) and (20) we can write ZT as.

$$\mathrm{ZT} = S^2 \mathrm{TG} \big/ K_e = \frac{S^2}{\mathrm{WF}}. \tag{21}$$

This equation shows that we can lead to cause an effective growth of ZT in regions where WF < 1 and at the same time $S > 1$. We found this optimum combination, within the temperature interval $T = [1–5]\Gamma$, at the weak coupling limit of the model, when the hybridization is low. In those regions, we obtain higher ZT values.

The thermoelectric properties are calculated following the standard textbook definitions [26,27]. In this way, the electrical conductance $G(T)$, the thermal conductance $K_e(T)$ and the thermopower (Seebeck effect) are defined by the relations respectively.

$$G(T) = e^2 I_o(T), \tag{22}$$

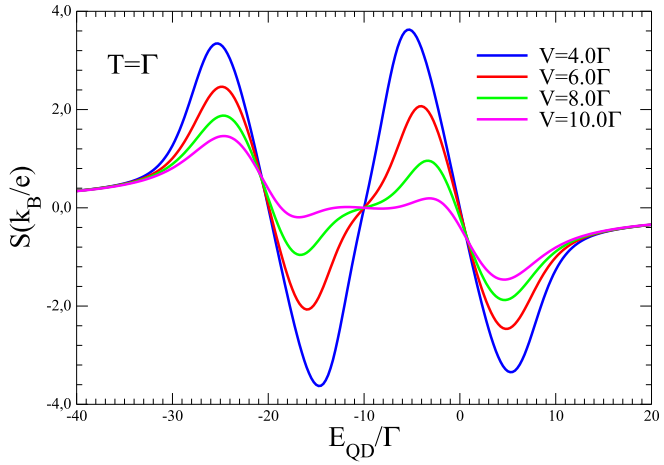

Fig. 2. Thermopower S vs. the gate voltage E_{QD} for different hybridizations V values, at temperature $T = \Gamma$.

$$K_e(T) = \frac{1}{T}\left(I_2(T) - \frac{I_1^2(T)}{I_o(T)}\right), \tag{23}$$

and.

$$S = \left(\frac{-1}{eT}\right)\frac{I_1(T)}{I_o(T)}. \tag{24}$$

To calculate the transport coefficients $I_o(T)$, $I_1(T)$, and $I_2(T)$, we follow the paper by Dong and X. L. Lei [28], which derived the particle current and thermal flux formulas, through an interacting QD connected to the leads, within the framework of the Keldysh non-equilibrium Green's functions (GF). The electric and thermoelectric transport coefficients were obtained in the presence of the chemical potential and temperature gradients with the Onsager relation in the linear regime automatically satisfied. The transport coefficients consistent with the thermoelectric general formulas derived earlier are given by.

$$I_n(T) = \frac{2}{h}\int\left(-\frac{\partial n_F(\omega,T)}{\partial\omega}\right)\omega^n\tau(\omega)\mathrm{d}\omega, \tag{25}$$

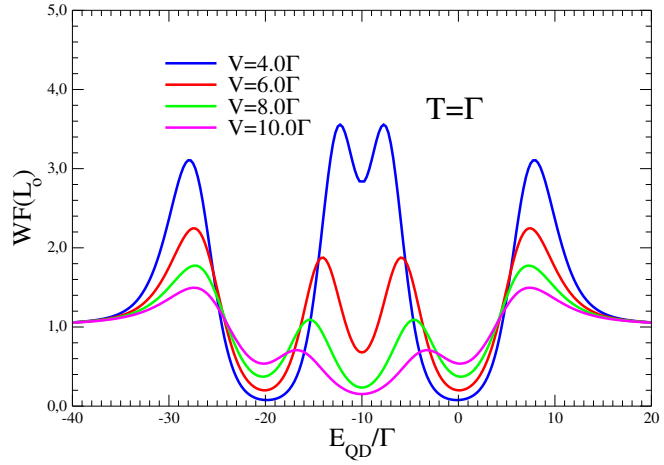

Fig. 3. The Wiedemann-Franz law WF vs. gate voltage E_{QD} for different hybridizations V and temperature $T = \Gamma$.

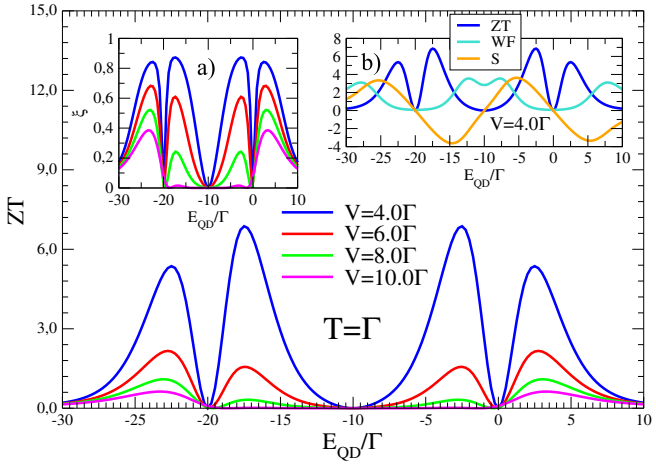

Fig. 4. Dimensionless thermoelectric figure of merit ZT vs. gate voltage E_{QD} for different hybridizations V and temperature $T = \Gamma$. In the inset a) of the figure we plot the parameter ξ. In the inset b) of the figure, we plot for $V = 4.0\Gamma$; the ZT values, the Wiedemann-Franz law WF and the thermopower S.

where $n_F(\varepsilon,T) = 1/(1+e^{(\varepsilon-\mu)/k_BT})$ is the Fermi-Dirac distribution, $\tau_\sigma(\omega) = (V^2/\Delta)^2\left|G_{00,\sigma}(\omega)\right|^2$ is the transmittance for the electrons with spin σ [30] and Δ is the Anderson parameter. $G_{00,\sigma}(\omega)$ is the local GF at the QD site, which for the immersed QD is

$$G_{00,\sigma}(\omega) = \left(G^c_\sigma(\omega)\right)^2V^2G^f_\sigma(\omega), \tag{26}$$

where the localized Green's function $G^f_\sigma(\omega)$ is calculated employing the atomic approach, and the conduction Green's function $G^c_\sigma(\omega)$, associated with the leads, is given by Eq. (10).

Following the work of G.D. Mahan and J. O. Sofo [20] we define the parameter ξ as a function of the thermoelectric coefficients.

$$\xi = \frac{I_1^2(T)}{I_o(T)I_2(T)}, \tag{27}$$

in terms of what the quantity ZT can be expressed. Employing Eqs. (22)–(24), the dimensionless thermoelectric figure of merit, defined from Eq. (1), can be written as

$$\mathrm{ZT} = \frac{\xi}{1-\xi}. \tag{28}$$

It is clear from the above equation that the best dimensionless thermoelectric figure of merit ZT occurs at the limit $\xi \to 1$. In the next section, we present the results for the ZT and the parameter ξ. We show that in the weak coupling regime of the SET, at temperatures above the Kondo temperature, it is possible to obtain ξ values close to 1, and in consequence the best thermoelectric efficiency.

5. Results and discussion

In our calculations, we employ the energy unit $\Gamma = 1$, where $D = 100\Gamma$ is the half-width of the conduction band and the chemical potential is always located at $\mu = 0$. The correlation U generates a two-level system: one level located at E_{QD} and the other at $E_{QD} + U$, which define the behavior of the thermoelectric properties of the SET. The electronic correlation energy U is given by $U = 20.0\Gamma$, and the symmetric limit of the Anderson model is attained when $E_{QD} = E_2 = -10.0\Gamma$. These parameters define two other energies: $E_1 = E_f - U/2 = -20.0\Gamma$ and $E_3 = E_f + U/2 = 0$. Those three energies are symmetrical points of the model. We restrict the

calculations of the present paper, to high temperature effects. This regime occurs approximately within the interval $T = [1-5]\Gamma$, and is characterized by strong charge fluctuations.

In Fig. 2 we show the thermopower S vs. the gate voltage E_{QD} for different hybridization values, at temperature $T = \Gamma$. The interesting point here is the increase of the thermopower with the decrease of the hybridization. The lower hybridization region (weak coupling limit), produces the most interesting results of the present paper, because the thermopower and the dimensionless thermoelectric figure of merit ZT attain high values [29]. This figure shows the particle-hole symmetry about the $S_{-E_{QD}} = -S_{E_{QD}}$ [16]. The oscillatory behavior of S is associated with the competition between the different charge carriers present in the system: electrons and holes. When $S < 0$ the dominant contribution to the thermopower is due to electrons and when $S > 0$ the dominant contribution is due to holes. The figure shows strong variations of the thermopower, mainly in the crossover from the empty dot to the single occupation region and in the crossover from the single occupation to the double occupation region. The two oscillations at around $E_{QD} = -10.0\Gamma$ are linked to heat transfer processes associated with charge fluctuations. Recently an experimental paper [11] has been published, that measures the thermopower of a quantum dot system in a temperature set ($T = 0.232$ K, $T = 1.5$ K, $T = 3.1$ K and $T = 6$ K) closer to our estimated temperature ($T = \Gamma \simeq 10$) K for our Fig. 2. Their thermopower results are shown in their Fig. 5a, and the general behavior of the curves is similar to that obtained by us in Fig. 2.

Fig. 3 shows the Wiedemann-Franz law, in Lorenz number L_o units vs. the energy E_{QD}, at various hybridizations values. At low temperatures, the Wiedemann-Franz law is always satisfied (we do not represent these curves here), but at high temperatures it is no longer valid, and the departure from its constant value, given by Eq. (20), shows a strong violation with the decrease of the hybridization.

In Fig. 4, we show the dimensionless thermoelectric figure of merit ZT vs. the gate voltage E_{QD} for different hybridizations V, and temperature $T = \Gamma$. As the hybridization decreases the violation of WF increases and for $V = 4.0\Gamma$, it exhibits the highest departure from its value at low temperatures. In inset a) of the figure we plot the parameter ξ, defined in Eq. (28), which exhibits regions of values close to one, and consequently great ZT values. In inset b) of the figure, we plot the ZT values, WF and the thermopower S for $V = 4.0\Gamma$.

It should be stressed that the violation of the WF does not lead to an automatic increase in ZT values. In Fig. 3, we observe that the maximum values of the WF occur at around the symmetric point $E_{QD} = -10.0\Gamma$, but the ZT values corresponding to this region, in Fig. 4 are very low. According to Eq. (1), high ZT values occur because for some E_{QD} values, there is a combination of lower values of WF and higher values of S at the same energy interval (see inset b) of the figure); both properties contribute in a complementary way to the ZT increase. The violation of the WF relation is intimately related to the variation of the parameter ξ, as indicated in inset b) of the figure.

In Fig. 5, we plot ZT as a function of the gate voltage E_{QD} for $V = 4.0\Gamma$ and different temperatures. For low hybridization and high temperatures we obtain a strong ZT value. At the same time, the inset shows that in the regions where ZT attains its maximum value, the parameter ξ is close to one. It should be stressed that in the ZT results presented in Figs. 4 and 5 we do not consider the phononic contribution, which tends to compete with the electronic contribution to decrease the ZT values, as the temperature is increased.

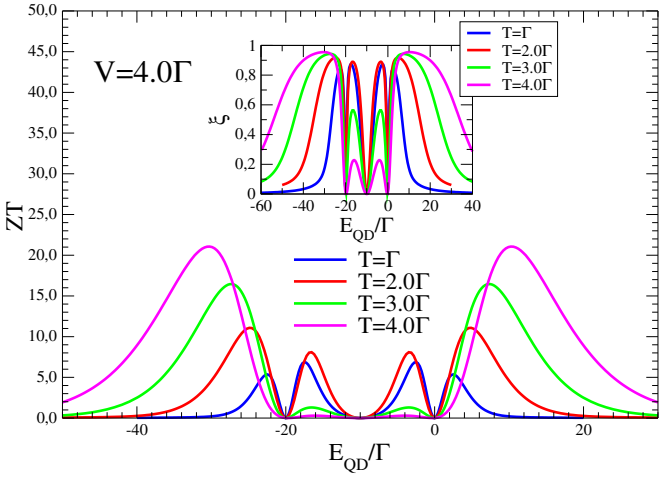

Fig. 5. Dimensionless thermoelectric figure of merit ZT vs. gate voltage E_{QD} for $V = 4.0\Gamma$ and different temperatures. In the inset we plot the parameter ξ vs. gate voltage E_{QD}.

6. Conclusions

We studied thermoelectric transport properties of the single electron transistor. The results obtained for the thermopower are consistent with a recent experimental paper [11]. Quantum dots, due to their sharp transmittance, can be considered an ideal nanoscopic system for producing large ZT's values, and one possible technological application of a single quantum dot may be to create localized cooling in nanoscopic systems [2]. Quantum dots have also been employed successfully for engineering quantum dot superlattices. In a recent paper Wang et al. [31] studied PbSe nanocrystal quantum dot superlattices varying nanocrystal sizes and they showed that for comparable carrier concentrations, PbSe nanocrystal superlattices exhibit a substantial thermopower enhancement relative to bulk PbSe.

According to Eq. (21), in order to produce an increase in ZT, it is necessary that the increase of the thermopower S be followed by a decrease in the WF at the same energy interval. We show that this condition is fulfilled at the weak coupling limit of the SET (low hybridizations) region, where the parameter ξ, introduced by G.D. Mahan and J. O. Sofo [20], is close to the unit. In this case ZT exhibits a strong increase. We show that the high values of ZT in those regions are associated with the violation of the Wiedemann-Franz law.

This result shows that the interesting region that could lead to practical applications of the system corresponds to temperatures within the interval $T = [1-5]\Gamma$. According to our previous estimate in the introduction of this paper, this energy interval approximately corresponds to $T \simeq [10-50]$ K, and can be attained using a helium liquid cryostat. In this region, the system shows strong charge fluctuations, mainly in the empty dot and the double occupation regions.

Acknowledgments

We are thankful for the financial support of DINAIN and DIB (Colombia National University), COLCIENCIAS (Colombia) and the Brazilian National Research Council CNPq. R. Franco and J. Silva-Valencia are grateful for the support of the International Centre for Theoretical Physics (ICTP)-Trieste, where part of this research was done.

References

[1] (a) L.D. Hicks, M.S. Dresselhaus, Phys. Rev. B 47 (1993) 12727;
(b) L.D. Hicks, T.C. Harman, M.S. Dresselhaus, Appl. Phys. Lett. 63 (1993) 3230.
[2] G. Chen, A. Shakouri, J. Heat Transf. 124 (2002) 242.
[3] Mildred S. Dresselhaus, Gang Chen, Ming Y. Tang, Ronggui Yang, Hohyun Lee, Dezhi Wang, Zhifeng Ren, Jean-Pierre Fleurial, Pawan Gogna, Adv. Mater. 19 (2007) 1043.
[4] Christopher J. Vineis, Ali Shakouri, Arun Majumdar, Mercouri G. Kanatzidis, Adv. Mater. 22 (2010) 3970.
[5] Jeannine R. Szczech, Jeremy M. Higgins, Song Jin, J. Mater. Chem. 21 (2011) 4037.
[6] Zhiting Tian, Sangyeop Lee and Gang Chen, arXiv:1401.0749v1 (2014).
[7] R. Scheibner, H. Buhmann, D. Reuter, M.N. Kiselev, L.W. Molemkamnp, Phys. Rev. Lett. 95 (2005) 176602.
[8] R. Scheibner, E.G. Novik, T. Borzenko, M. König, D. Reuter, A.D. Wieck, H. Buhmann, L.W. Molenkamp, Phys. Rev. B 75 (2007) 041301.
[9] R. Scheibner, M. König, D. Reuter, A.D. Wieck, C. Gould, H. Buhmann, L.W. Molenkamp, New. J. Phys. 10 (2008) 083016.
[10] Eric A. Hoffmann, Henrik A. Nilsson, Jason E. Matthews, Natthapon Nakpathomkun, Ann I. Persson, Lars Samuelson, Heiner Linke, Nano Lett. 9 (2009) 779.
[11] S. Fahlvik Svensson, A.I. Persson, E.A. Hoffmann, N. Nakpathomkun, H.Q. Xu, H.A. Nilsson, H.Q. Xu, L. Samuelson, H. Linke, New. J. Phys. 14 (2012) 033041.
[12] Olli-Pentti Saira, M. Meschke, F. Giazotto, A.M. Savin, M. Möttonen, J.P. Pekola, Phys. Rev. Lett. 99 (2007) 027203.
[13] Noah Linden, Sandu Popescu, Paul Skrzypczyk, Phys. Rev. Lett. 105 (2010) 130401.
[14] Pramod Reddy, Sung-Yeon Jang, Rachel A. Segalman, Arun Majumdar, Science 315 (2007) 1568.
[15] M. Yoshida, L.N. Oliveira, Phys. B 404 (2009) 3312.
[16] T.A. Costi, V. Zlatić, Phys. Rev. B 81 (2010) 235127.
[17] D. Goldhaber-Gordon, J. Gores, H. Shtrikman, D. Mahalu, U. Meirav, M.A. Kastner, Mater. Sci. Eng. B84 (2001) 17.
[18] W.G. van der Wiel, S. De Franceschi, T. Fujisawa, J.M. Elzerman, S. Tarucha, L.P. Kouwenhoven, Science 289 (2000) 2105.
[19] Andrey V. Kretinin, Hadas Shtrikman, David Goldhaber-Gordon, Markus Hanl, Andreas Weichselbaum, Jan von Delft, Theo Costi, Diana Mahalu, Phys. Rev. B 84 (2011) 245316.
[20] G.D. Mahan, J.O. Sofo, Proc. Natl. Acad. Sci. USA 93 (1996) 7436–7439.
[21] (a) X. Zianni, J. Electron. Mater. 39 (2010) 1996;
(b) X. Zianni, Phys. Rev. B 82 (2010) 165302.
[22] John S. Blakemore (Ed.), Key Papers in Physics:Gallium Arsenide, AIP Physics, New York, 1987.
[23] Jie Ren, Jian-Xin Zhu, James E. Gubernatis, Chen Wang, L. Baowen, Phys. Rev. B 85 (2012) 155443.
[24] T. Lobo, M.S. Figueira, M.E. Foglio, Nanotechnology 21 (2010) 274007.
[25] M.E. Foglio, T. Lobo, M.S. Figueira, AIP Adv. 2 (2012) 032139.
[26] Gerald D. Mahan, Many-Particle Physics, second ed., Chap. 3, p. 227.
[27] J. M. Ziman, Principles of the Theory of Solids, second ed., chap. 7 pg. 229.
[28] B. Dong, X.L. Lei, J. Phys. Condens. Matter 14 (2002) 11747.
[29] R. Franco, J. Silva-Valencia, M.S. Figueira, J. Mag. Mag. Mat. 320 (2008) 242.
[30] K. Kang, S.Y. Cho, J.J. Kim, S.C. Shin, Phys. Rev. B 63 (2001) 113304.
[31] Robert Y. Wang, Joseph P. Feser, Jong-Soo Lee, Dmitri V. Talapin, Rachel Segalman, Arun Majumdar, Nano Lett. 8 (2008) 2283.